Dispersion of Gold Nanoparticles in UV-Cured, Thiol−Ene Films by Precomplexation of Gold−Thiol

J. Paige Phillips,*,† Nicole M. Mackey,† Bridget S. Confait,† David T. Heaps,† Xiao Deng,† Meredith L. Todd,† Steven Stevenson,† Hui Zhou,‡ and Charles E. Hoyle‡

Department of Chemistry and Biochemistry, and School of Polymers and High Performance Materials, University of Southern Mississippi, 118 College Drive, Hattiesburg, Mississippi 39406

Received March 17, 2008. Revised Manuscript Received May 12, 2008

Alkyl thiols and alkenes (enes) polymerize via an extremely rapid step-growth, free-radical chain process, uninhibited by air, to give high-density networks with excellent mechanical and physical properties. These thiol−ene coatings are potentially useful for a wide variety of coatings, adhesives, and optical applications. In this work, a series of nanogold-containing UV-cured, thiol−ene coatings were prepared from trimethylolpropane tris(3-mercaptopropionate) (trithiol) and pentaerythritol allyl ether (triene) monomers using a unique procedure which facilitates precomplexation of the gold−thiol prior to photocuring. Irgacure 651 (1 wt %) was used as a photoinitiator, and nanogold was incorporated at 0−1 wt %, average ∼10 nm size particles by TEM. Physical and mechanical properties were characterized using bulk tack analysis and other standard techniques: DSC, TGA, pencil hardness, and gel fractions. In general, films were found to be low absorbing in the visible range and highly uniform and to contain well-dispersed nanogold particles. Although the rate of polymerization was modestly retarded by the presence of gold nanoparticles, functional group conversions (C═C and S−H) and gel fractions were high. Increasing nanogold content resulted in an increase in T_g measured by DSC (−15 to −8 °C for 0−1 wt % nanogold, respectively) due to the increasing number of physical gold−thiol cross-links created. TGA analysis revealed a small negative impact of increasing nanogold composition on relative thermal stability. The 1 wt % nanogold-containing samples possessed appreciable electrostatic discharge (ESD) character, with ESD times of 1−10 s measured using a commercial charge plate analyzer.

1. Introduction

The area of polymeric nanocomposites has received intense activity in the past 15 years,[1] and the blending of nanometer-scale fillers has resulted in significant improvements in bulk polymer composite properties, e.g., barrier properties, corrosion resistance, and conductivity. Although there are a large number and variety of reports in the literature on the use of polymers as stabilizers in the synthesis of well-dispersed, functional gold nanoparticles,[2–12] few reports of well-defined polymer−nanogold composites exist.[13–19] The polymer constituent element of the nanocomposite in these reports varies among poly(methylphenylphosphazene),[19] poly(2-hydroxyethyl methacrylate),[17] polyurethane,[15] polystyrene,[14,16] poly(ethylene glycol),[14] poly(amic acid),[13] and polyimide.[18]

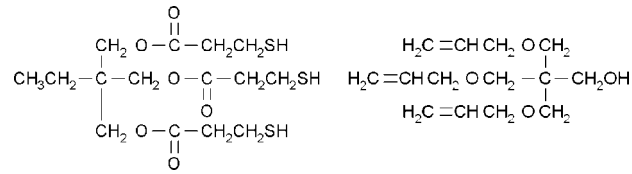

Figure 1. Chemical structures of monomers (left) trimethylolpropane tris(3-mercaptopropionate) (trifunctional thiol) and (right) pentaerythritol allyl ether (trifunctional ene).

Mixtures of multifunctional thiols and enes, e.g., Figure 1, readily polymerize to give high-density networks with excellent mechanical and physical properties.[20–23] Since such thiol−ene systems cure by an extremely rapid step-growth,

* To whom correspondence should be addressed. Phone: (601) 266−4083. Fax: (601) 266−6075. E-mail: janice.phillips@usm.edu.
† Department of Chemistry and Biochemistry.
‡ School of Polymers and High Performance Materials.

(1) Vaia, R.; Maguire, J. *Chem. Mater.* **2007**, *19*, 2736.
(2) Carroll, J. B.; Frankamp, B. L.; Rotello, V. M. *Chem. Commun.* **2002**, 1892.
(3) Corbierre, M. K.; Cameron, N. S.; Sutton, M.; Mochrie, S. G. J.; Lurio, L. B.; Ruhm, A.; Lennox, R. B. *J. Am. Chem. Soc.* **2001**, *123*, 10411.
(4) Frankamp, B. L.; Boal, A. K.; Rotello, V. M. *J. Am. Chem. Soc.* **2002**, *124*, 15146.
(5) Frankamp, B. L.; Uzun, O.; Ilhan, F.; Boal, A. K.; Rotello, V. M. *J. Am. Chem. Soc.* **2002**, *124*, 892.
(6) Kamata, K.; Lu, Y.; Xia, Y. N. *J. Am. Chem. Soc.* **2003**, *125*, 2384.
(7) Mandal, T. K.; Fleming, M. S.; Walt, D. R. *Nano Lett.* **2002**, *2*, 3.
(8) Norsten, T. B.; Frankamp, B. L.; Rotello, V. M. *Nano Lett.* **2002**, *2*, 1345.
(9) Shimmin, R. G.; Schoch, A. B.; Braun, P. V. *Langmuir* **2004**, *20*, 5613.
(10) Spatz, J. P.; Mossmer, S.; Moller, M. *Chem.-Eur. J.* **1996**, *2*, 1552.
(11) Spatz, J. P.; Roescher, A.; Moller, M. *Adv. Mater.* **1996**, *8*, 337.
(12) Teranishi, T.; Kiyokawa, I.; Miyake, M. *Adv. Mater.* **1998**, *10*, 596.
(13) Andreescu, D.; Wanekaya, A. K.; Sadik, O. A.; Wang, J. *Langmuir* **2005**, *21*, 6891.
(14) Corbierre, M. K.; Cameron, N. S.; Sutton, M.; Laaziri, K.; Lennox, R. B. *Langmuir* **2005**, *21*, 6063.
(15) Hsu, S. H.; Chou, C. W.; Tseng, S. M. *Macromol. Mater. Eng.* **2004**, *289*, 1096.
(16) Huang, H. M.; Chang, C. Y.; Liu, I. C.; Tsai, H. C.; Lai, M. K.; Tsiang, R. C. C. *J. Polym. Sci., Part A: Polym. Chem.* **2005**, *43*, 4710.
(17) Kariuki, N. N.; Han, L.; Ly, N. K.; Patterson, M. J.; Maye, M. M.; Liu, G. J.; Zhong, C. J. *Langmuir* **2002**, *18*, 8255.
(18) Maggioni, G.; Vomiero, A.; Carturan, S.; Scian, C.; Mattei, G.; Bazzan, M.; Fernandez, G. D.; Mazzoldi, P.; Quaranta, A.; Della Mea, G. *Appl. Phys. Lett.* **2004**, *85*, 5712.
(19) Walker, C. H.; St John, J. V.; Wisian-Neilson, P. *J. Am. Chem. Soc.* **2001**, *123*, 3846.

10.1021/cm8007842 CCC: $40.75 © 2008 American Chemical Society
Published on Web 07/30/2008

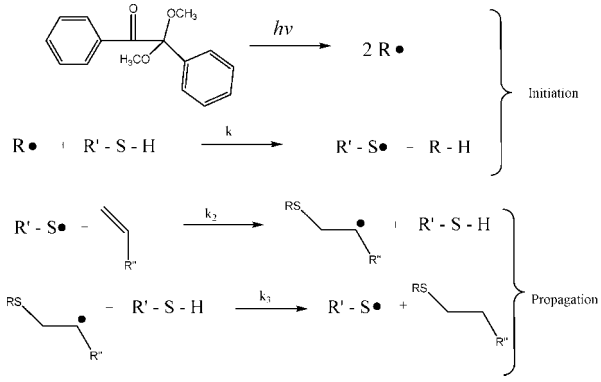

Figure 2. Initiation and propagation steps of the thiol−ene step-growth, free-radical chain process, using Irgacure 651 as a cleavage photoinitiator.

free-radical chain process in the presence of air, they can potentially be used for a wide variety of coatings, adhesives, and optical applications.[21,22] Generic initiation and propagation steps of the step-growth, free-radical chain process are shown in Figure 2, using Irgacure 651 as a cleavage photoinitiator. It has been demonstrated that thiol−ene based networks are extremely uniform, leading to mechanical and thermal transformations at the glass transition over very narrow glass transition ranges. Hence, these uniformly structured networks can be tuned to exhibit an extremely wide range of properties depending upon the chemical structures of the thiols and enes. Since thiols readily add to virtually any terminal double bond (i.e., ene), it is possible to select a combination of ene structures that allow precise tuning of a set of physical, mechanical, thermal, and optical properties. Due to the affinity of thiols to bind to gold surfaces, it is expected that thiol−ene systems should be excellent network structures for stabilizing well-dispersed gold nanoparticles, and such systems would have potential use as magnetically and electrically active networks.

As electronic components become more advanced, so does the need to protect static-sensitive components from the buildup of electrostatic charge. Coatings capable of preventing or inhibiting static buildup (ESD) must meet two basic requirements: (1) they must not contribute to static buildup and (2) must be groundable. In this process, the charges generated from the friction of two (usually dissimilar insulating) materials at the substrate surface are channeled away to a conductor and prevented from accumulating. Herein, we describe the preparation of a series of thiol−ene coatings containing 0−1 wt % nanogold using a unique procedure, which enables precomplexation of the gold−thiol prior to photocuring. The thiol monomer functions simultaneously to affect dispersion of the gold particles and to be a reagent in the thiol−ene curing reaction. Of particular interest to us is characterizing the impact of the gold−thiol interaction on the rate of photopolymerization with increasing additive. The physical and mechanical properties of the resulting films are characterized using standard techniques, and the samples are evaluated for ESD capabilities.

2. Experimental Section

2.1. Materials. Trimethylolpropane tris(3-mercaptopropionate) (trithiol, 96−99%), pentaerythritol allyl ether (triene, 70%; remaining 30%, monoene), and gold nanopowder (99.9+%) were purchased from Aldrich and used as received. Irgacure 651 was purchased from Ciba Specialty Chemicals Corps and also used without further purification.

2.2. Film Preparation. Trithiol and triene concentrations were held constant at 1:1 mol equiv in the following procedure. A known mass of gold nanoparticles was added to the trithiol to achieve a series of weight percents of gold in the final resulting thiol−ene films ranging from 0.01 to 1.0 wt %. The gold−thiol mixtures were alternatively sonicated and stirred in 1 h increments for approximately 5 h, before being stirred continuously for several days until no particles could be observed to settle out upon standing. Stirring time required to evenly disperse the gold nanoparticles in thiol monomer increased as gold content increased. The two benchmarks 0.01 and 1.0 wt % gold content required roughly 1 and 3 weeks agitation, respectively. When the gold was evenly dispersed—as determined by a resulting clear, faint blue-gray solution—the triene was added to the gold−thiol dispersion along with 1 wt % of Irgacure 651 photoinitiator. The final sample was covered with aluminum foil to block any light exposure and was stirred for an additional 15 min before use. In general, films were drawn on clean glass plates from the prepared 100% solids solution using the eight-path wet film applicator (Paul N. Gardner Co.) on #2. Radiation curing of films was performed on a Fusion System Corporation Epiq 6000 UV system, 1.095 W/cm^2. Ten films were prepared from each sample to allow variation of light exposure, as controlled by the number of passes through the cure line. The cured films had a thickness of 30−35 μm.

2.3. Bulk Tack and Pencil Hardness. Film tack of samples prepared on glass plates was monitored using a TA XTplus Texture Analyzer (Godelming, Surrey, UK). With use of compression test mode, the applied force required to penetrate 10% of the film thickness with a 1 in. round probe tip at a probe insertion speed of 0.1 mm/s was determined for a cured sample, 72 g. In tack measurements the probe tip and applied force was held for 10 s, and then the probe tip was withdrawn at a constant rate from the film of 0.1 mm/s. Force measurements are recorded as grams per unit time, and the highest force point is recorded as the peak force. Pencil hardness tests were also performed—according to ASTM method D 3363 00—where the degree of hardness of a pencil used to scratch the film surface at a 45 ° angle in a 0.25 in. stroke is systematically increased until the pencil visually mars the film surface. The hardest pencil that will not scratch the surface is determined from the scale of 9B to 9H, with 9B and 9H being the softest and hardest leads, respectively.

2.4. Mechanical, Thermal Analysis, and Gel Fractions. Glass transition temperatures (T_g) of prepared polymer samples were measured using a TA Instruments #2920 Modulated Differential Scanning Calorimeter (DSC) instrument. Cured samples were removed from glass plates and cut into ∼10 mg test samples. Samples were monitored over the temperature range of −50 to 50 °C in a heat/cool/heat cycle at 10 °C/min. T_g information was taken from the second heating cycle. Gel fractions of the cured films were obtained by dissolving a known mass of film in chloroform, resting the sample for 24 h at room temperature, and recovering the

(20) Hoyle, C. E.; Lee, T. Y.; Roper, T. *J. Polym. Sci., Part A: Polym. Chem.* **2004**, *42*, 5301.
(21) Jacobine, A. In *Radiation curing in polymer science and technology III: polymerization mechanisms*; Fouassier, J., Rabek, J., Eds.; Elsevier: London, 1993; Chapter 7.
(22) Morgan, C.; Magnotta, F.; Ketley, A. *J. Polym. Sci., Part A: Polym. Chem.* **1977**, *15*, 627.
(23) O'Brien, A. K.; Cramer, N. B.; Bowman, C. N. *J. Polym. Sci., Part A: Polym. Chem.* **2006**, *44*, 2007.

insoluble mass fraction, followed by residual solvent evaporation under reduced pressure. The thermal stability of cured polymer samples was evaluated by thermogravimetric analysis (TGA) where weight changes in a material are monitored as a function of temperature (or time) under a controlled atmosphere. With use of a TA instruments #2050 series TGA instrument, average 10 mg samples were analyzed in platinum pans over the temperature range of 0−600 °C at a heating rate of 20 °C/min. The degradation onset temperature was determined at 10% mass loss.

2.5. UV−Vis and Real-Time Infrared. The absorbance spectra over visible wavelengths were obtained for prepared ca. 30 μm films on quartz slides using a Shimadzu Corp. UV-2401 PC Spectrophotometer. Real-time infrared (RTIR) spectra were recorded on a modified Bruker 88 spectrometer. UV light from an Oriel lamp system equipped with a 200 W, high-pressure mercury−xenon bulb was channeled through an electric shutter and fiber optic cable in the sample chamber filled with dry air. The photopolymerizations were conducted in a cell prepared by sandwiching the samples between two sodium chloride salt plates with a thickness of approximately 20 μm. Photopolymerizations were conducted upon exposure to the UV light at intensities of 1.87 mW/cm^2. (The light intensity was measured with an IL-1400 calibrated radiometer from International Light.) Infrared absorption spectra were obtained under continuous UV irradiation at a scanning rate of 5 scans/s. The characteristic infrared absorbance bands used to monitor the disappearance of the monomers during the photoreactions were as follows: allyl ether (3080 cm^{-1}) and thiol group (2570 cm^{-1}).

2.6. TEM Imaging. Representative UV-cured, thiol−ene films containing 1 wt % gold nanoparticles were embedded into Spurr's Low Viscosity embedding mixture and cured at 70 °C for 36 h. Ultrathin cuts were obtained by a Sorvall, Porter Blum ultramicrotome with glass knives and applied to copper grids. The thickness of the sections was approximately 10 μm. Glass knives were prepared from ultra glass knife strips purchased from Electron Microscopy Sciences and cut using a LKB Knifemaker type 7801 B. TEM images were taken on a Zeiss High-Resolution Electron Microscope EM 10C/CR operated at 50 kV and at a magnification of 30 and 140k.

2.7. ESD Measurements. Electrostatic discharge measurements were conducted on a Monroe Electronics Charge Plate Analyzer, Model 268A-1, using manufacturer suggested protocols. Coatings were cast as previously described to completely cover ITO-coated glass substrates. Samples were charged to 1.1 kV on the coating side, and the time required for the sample voltage to drop from 1 kV to 100 V (90% decrease) was measured in seconds. ESD values of 0.8−0.9 s were obtained on the uncoated substrate. Room humidity was controlled at 30% R.H.

3. Results and Discussion

The changes in thermal, mechanical, and physical properties of UV-cured, thiol−ene films were measured as a function of increasing gold nanoparticle content. In general, films were prepared from equal molar amounts of trithiol and triene, 1 wt % Irgacure 651 photoinitiator, and 0.01−1 wt % gold nanoparticles, and representative films are illustrated in Figure 3. The precomplexation of the gold nanoparticles to thiol monomer was found to be critical to successful film formation, producing uniform transparent and only faintly colored films at 30−35 μm thickness. The visible absorbance spectrum is provided in Figure 4 and supports the low-absorbing characteristic of the films over the visible wavelength range and 0−1 wt % nanogold content. Note that Figures 3 and 4 suggest gold particle aggregation at 1.0 wt %.

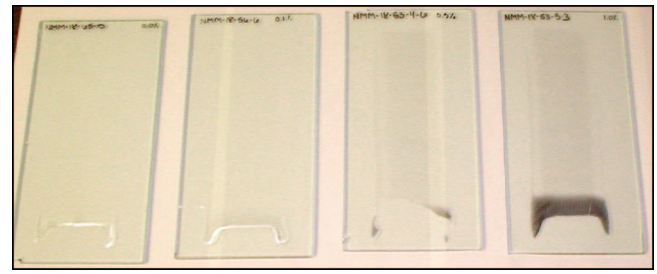

Figure 3. Representative UV-cured, thiol−ene films containing 0, 0.1, 0.5, and 1.0 wt % gold nanoparticles and film sample thickness of 30−35 μm.

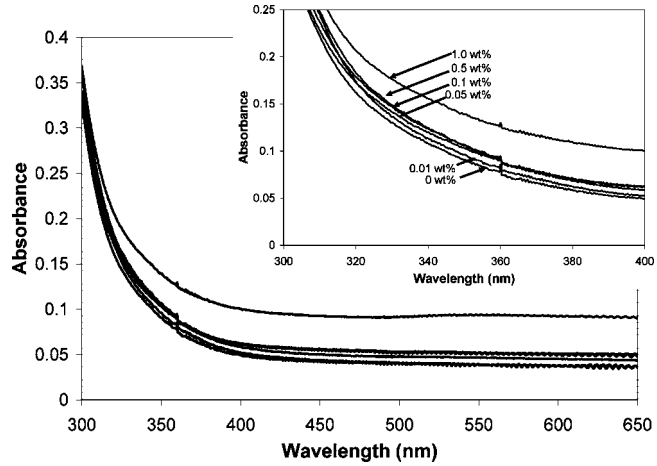

Figure 4. UV−vis spectra 300−650 nm (300−400 nm insert) of prepared ≈0.35 μm gold−thiol−ene films on quartz slides at 0, 0.01, 0.05, 0.1, 0.5, and 1.0 wt % loading gold nanoparticles.

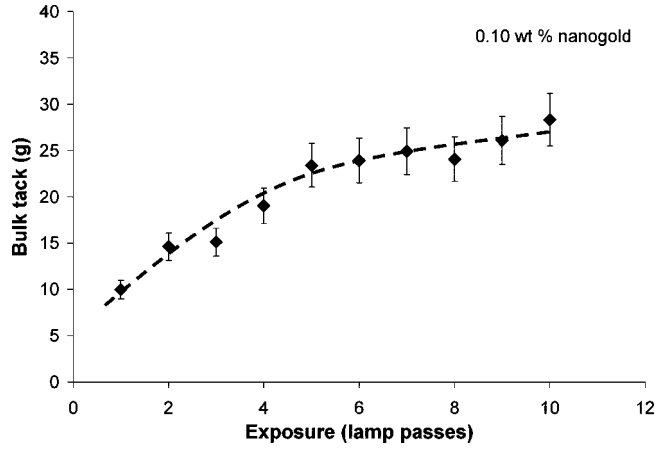

Figure 5. Representative sample bulk tack dependence on lamp exposure time, 0.10 wt % nanogold in thiol−ene film; first fully cured sample estimated at 5 lamp passes; and plateau bulk values determined from average ≥5 lamp passes.

Physical and mechanical testing was performed only on fully cured samples. Bulk tack analysis was used to monitor cured films as a function of radiation exposure, and a representative bulk tack analysis is provided in Figure 5. Bulk tack or alternatively film hardness data offers unique advantages to approximate a rough rate of cure (initial slope) and determine when film physical properties became constant (plateau region). The technique is simple and does not require

Table 1. Characterization of Gold−Thiol−Ene Film Mechanical Properties and Relative Thermal Stability

sample ID (wt %)[a]	pencil hardness[b]	bulk tack (g)[c]	gel fraction (wt %)[d]	glass transition temperature, T_g (°C)[e]	thermal degradation onset (°C)[f]
0	2H	18 (±2)	90	−15	372.9
0.01	H	18 (±2)	93	−13	371.3
0.05	H	23 (±2)	89	−12	371.0
0.1	H	25 (±2)	93	−9	367.2
0.5	H	21 (±1)	90	−8	365.5
1	H	22 (±3)	92	−8	365.9

[a] Weight percent of gold nanoparticles in film. [b] According to pencil hardness test: ASTM method D 3363 00. [c] Gram force required to remove a stainless steel 1 in. probe tip penetrated 10% thickness of cured coating and held for 10 s (stand. dev. of five samples). [d] Insoluble mass fraction recovered after 24 h solvent exposure. [e] T_g recorded as inflection point of step transition in the second heating DSC cycle. [f] Calculated from TGA data as the temperature corresponding to 10% mass loss.

sample removal from the substrate or necessitate a secondary spectroscopic characterization technique. In this process, films are secured on a stage, and a 1 in. stainless steel round probe is inserted into the film 10% of film thickness, held for 10 s, and then removed at a constant rate. The instrument records the amount of force required to pull the probe tip away in grams force per unit time. Bulk tack values of gold−thiol−ene films became approximately consistent after 5 lamp passes, and therefore these samples were used in further physical and mechanical characterization.

Table 1 summarizes the mechanical, physical, and relative thermal stabilities of the prepared films. Pencil hardness tests determined that films were comparable in scratch resistance over the range of gold nanoparticle compositions studied. A similar result was observed in plateau bulk tack values. Interestingly, films were found to possess slightly lower bulk tack at < 0.01 wt % nanogold, suggesting that at nanogold ≥0.01 wt % there is a small but contributing effect of gold incorporation to the measured physical properties of the prepared films. Above 0.01 wt % bulk tack is independent of nanogold content. Gel fractions were obtained, and the insoluble mass fractions of films after 24 h solvent exposure were high (low 89.3% to high 93.3%), indicating extensive cross-linking.

Nanogold composition was found to have a dramatic impact on glass transition temperatures determined by differential scanning calorimetry (DSC) and thermal degradation onset temperatures using thermogravimetric analysis (TGA). Glass transition temperatures (T_g) were determined as the inflection point in the temperature step of the DSC plots shown in Figure 6 and are reported in Table 1. An obvious trend of T_g with increasing nanogold content was observed, ranging from −15 to −8 °C at 0 and 1 wt %, respectively. The T_g did not increase from 0.5 wt % to 1.0 wt % gold: which is consistent with the aggregation noted previously. A 7 °C increase in T_g is significant and supports the active role of nanogold particles in network formation. Increasing gold content has the effect of increasing the basic network rigidity by the development of a number of physical contact sites between gold nanoparticles and the matrix. Similar results were demonstrated recently by Xiao and Gao[24] and Krakovsky et al.[25] Xiao and Gao[24] prepared a series of physically cross-linked complex hydrogels of poly(vinyl alcohol) (PVA) and sodium carboxymethylcellulose (CMC). When analyzed by DSC, the glass transition

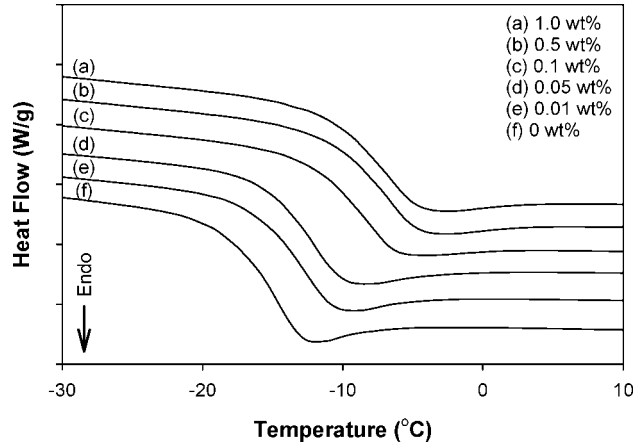

Figure 6. DSC analysis of UV-cured, gold−thiol−ene film samples with increasing nanogold content and sample thickness of 30−35 μm.

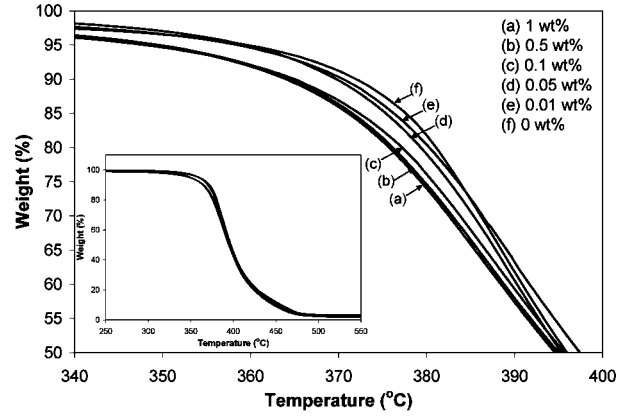

Figure 7. TGA analysis of UV-cured, gold−thiol−ene film samples with increasing nanogold content.

temperature of polymer hydrogels increased with increasing content of the CMC physical cross-linker. The structure and molecular dynamics of α,ω-dihydroxy terminated polybutadienes of varying number averaged molecular weight (1320−10500 g/mol) were investigated by Krakovsky et al.[25] DSC results supported a physically linked network among clusters of H-bonded end groups, where T_g increased upon decreasing molecular weight between end groups.

TGA analysis monitors weight loss with time and temperature, and representative TGA plots of cured gold−thiol−ene films are provided in Figure 7. Thermal degradation onset temperatures were calculated and reported in Table 1 as the temperature corresponding to 10% mass loss. At the two nanogold composition extremes, 0 and 1 wt %, thermal degradation onset temperatures were determined to be ca. 373 and 366 °C, indicating a negative influence of

(24) Xiao, C. M.; Gao, Y. K. *J. Appl. Polym. Sci.* **2008**, *107*, 1568.
(25) Krakovsky, I.; Hanykova, L.; Trchova, M.; Baldrian, J.; Wubbenhorst, M. *Polymer* **2007**, *48*, 2079.

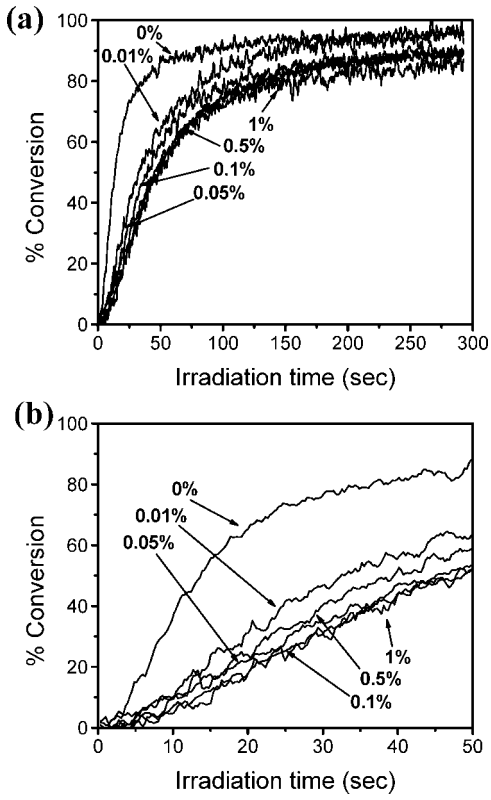

Figure 8. (a) Real-time FTIR analysis of C═C conversion as a function of irradiation time for UV-cured, gold−thiol−ene film samples containing 0, 0.01, 0.05, 0.1, 0.5, and 1.0 wt % gold nanoparticles; (b) expanded to reflect initial rates.

nanogold composition on relative thermal stability. This is not surprising given the previous literature on the catalytic ability of gold nanoparticles to promote the thermal decomposition of their constituent nanocomposite polymers,[16,19,26] and in many compositions this effect can be dramatic, i.e., hundreds of degrees at low loadings of nanogold. In the case of our gold−thiol−ene nanocomposite films, there is minimal decreased thermal stability up to 1 wt % of nanogold.

Real-time FTIR analysis of ca. 20 μm gold−thiol−ene films were investigated over the concentration range of 0−1 wt% nanogold. During photoreactions, the absorbance bands corresponding to monomers—allyl ether (3080 cm^{-1}) and thiol group (2570 cm^{-1})—were monitored as a function of time, and rates of functional group conversion were determined from plotted results. This in situ IR technique allows for accurate monitoring of IR band intensities since the analysis is performed on the same sample in exactly the same spot at various irradiation times. Film exposure was performed using a high-pressure, mercury−xenon UV source. Functional group conversion was determined to be equivalent for thiol or ene functional groups. Representative plots of C═C conversion as a function of irradiation time are shown in Figure 8a and expanded in Figure 8b to reflect differences in initial rates among the gold series. Rates of polymerization (Rp, s^{-1}) were calculated as initial rates from the slope of the C═C percent conversion versus time plot at low percent conversion. Rp values along with reaction C═C % conversions are summarized in Table 2. There is a significant retardation of the rate of photopolymerization from 0 to 0.01 wt % gold; however, ultimately high percent C═C conversions of 96% are obtained in both cases. There is a subtle decreasing percentage conversion in the series of samples from 0.01 to 1 wt % nanogold of 96 to 87%, respectively, and is attributed to the increased gold−thiol interactions and consequently decreased thiol availability at high gold concentrations. Rp is independent of gold concentration above 0.01 wt %. The influence of nanogold on the Rp from 0 to 0.01 wt % was determined to be a kinetic effect resulting from the presence of strong thiol−gold interactions, not a filtering effect due to less light transmission through the sample. The greatest retarding on the Rp (0−0.01 wt%) corresponds to the samples with the lowest increase in UV−vis absorbance; conversely, the most significant change in absorbance from 0.5 to 1 wt % nanogold corresponds to an insignificant change in Rp.

Table 2. Effect of Gold Concentration on Photopolymerization Kinetics and C═C Conversion in Gold−Thiol−Ene Films

sample ID[a]	rate of polymerization (Rp, s^{-1})[b]	% conversion
0 wt %	4.1	96
0.01 wt %	1.7	96
0.05 wt %	1.2	90
0.1 wt %	1.2	89
0.5 wt %	1.5	89
1 wt %	1.2	87

[a] Weight percent of gold nanoparticles in film. [b] Initial slope of % conversion versus time plot.

A primary motivation for performing this work was to determine if the advantages of thiol−ene photopolymerization chemistry (100% solids system, plethora of commercially available monomers, photopolymerization in the presence of O_2, low shrinkage, and uniform network structure) could be utilized in the preparation of coatings having enough conductivity to produce electrostatic discharge coatings. The ESD capabilities were measured on the gold−thiol−ene coatings prepared during this effort, and only 1 wt % coatings had sufficient ESD. ESD values for 1 wt % gold−thiol−ene coatings ranged from 1 to 10 s, and ESD times increased dramatically as gold content decreased. The 1 wt % nanogold loading is below the value predicted by the percolation theory of perfectly dispersed particles to afford appreciable conductivity; therefore, the ESD results obtained in this study are attributed to particle aggregation, which may be further enhanced upon film charging to the required 1.1 kV for testing. Films prepared with >1 wt% nanogold—although having lower ESD times—were no longer considered low-absorbing coatings and in extreme cases were complicated by nanogold aggregation and precipitation during preparation. Finally, transmission electron microscopy (TEM) analysis was performed on select compositions to optically interrogate the distribution of gold nanoparticles within the thiol−ene matrix. Samples were prepared and microtomed for testing using standard techniques. Representative 1.0 wt % gold−thiol−ene images are provided in Figure 9 and illustrate the distribution and size of gold nanoparticles within the films. In general, gold nanoparticles are distributed well within the matrix and no large agglomerates were observed.

(26) Chang, C. M.; Chang, C. C. *Polym. Degrad. Stab.* **2008**, *93*, 109.

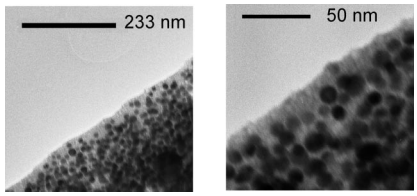

Figure 9. Representative TEM images of UV-cured, gold−thiol−ene films containing 1 wt % gold nanoparticles.

4. Conclusions

The significant advantages of UV-cure, thiol−ene coatings chemistry were combined with the intrinsic gold−thiol affinity to prepare a series of nanogold-containing UV-cured coatings from a trifunctional thiol and trifunctional ene. The methodology used enables precomplexation of the gold−thiol prior to photocuring to produce uniform coatings, which are low-absorbing in the visible range and contain well-dispersed nanogold particles. Increasing nanogold content from 0 to 1 wt % was observed to increase the T_g and slightly decrease relative thermal stability. Functional group conversions and gel fractions were high; however, the rate of polymerization was significantly retarded by the presence of gold nanoparticles. Samples were evaluated for potential ESD applications, and only the 1 wt % nanogold-containing samples possessed appreciable ESD character, with ESD times of 1−10 s measured using a commercial charge plate analyzer. Ongoing research continues to improve coating properties and decrease ESD times.

Acknowledgment. This work was supported primarily by the MRSEC Program of the National Science Foundation under Award Number DMR-0213883. Additional support from the Department of Education GAANN Fellowship Award #P200A060323 and the University of Southern Mississippi New Faculty Start-Up is gratefully acknowledged.

CM8007842